Iranian Journal of Materials Science & Engineering Vol. 16, No. 2, June 2019

RESEARCH PAPER

Effect of Si and Al on the Microstructure, Mechanical Properties and Machinability of 65Cu-35Zn Brass

M. Adineh, H. Doostmohammadi* and R. Raiszadeh

* *hd@uk.ac.ir*

Received: March 2018 **Revised: September 2018** **Accepted: January 2019**

Department of Metallurgy and Materials Science, School of Engineering, Shahid Bahonar University of Kerman, Kerman, Iran.

DOI: 10.22068/ijmse.16.2.21

Abstract: *Relations between the microstructure, mechanical properties and machinability of as-cast 65Cu-35Zn brass with various amounts of Al (1.89, 3.65 and 4.72 wt%) and Si (0, 0.83, 1.87, 2.28 and 3.62 wt%) were investigated. Both Si and Al initially enhanced the ultimate tensile strength (UTS) and toughness of the brass samples, which led to an improvement in machinability due to a reduction in the main cutting force. A duplex brass with randomly oriented α plates in β' matrix was found to have the best machinability among the other microstructures. It was found that besides the presence of brittle phases, such as β' phase in the microstructure, the morphology and hardness of the phases involved had a significant influence on machinability.*

Keywords: *Brass, Silicon, Aluminum, microstructure, machinability.*

1. INTRODUCTION

Aluminum brass alloys are utilized in water distribution systems, seawater services, manufacturing of condensers and heat exchangers due to their excellent resistivity to oxidation and corrosion [1, 2]. Moreover, aluminum addition can lead to a decrease in the oxidation of zinc during casting due to the formation of a protective oxide layer on the surface of the melting brass [3]. The Cu-Zn-Al alloys are also well-known for their shape memory effect, excellent electric performance, appropriate heat conductivity, and easy manufacturing. They have the potential for use in the biomedical, automotive, aerospace and microsystems industries [4-6].

Lead is added to brasses to improve their machinability through a reduction in cutting force and better chip breakage [7]. This element, however, is toxic and harmful to human health. Silicon has been introduced as a substitute for Pb in brass alloys [8-10] since various pieces of legislation have been validated to prohibit or decrease the consumption of lead in different countries and for different applications.

Brass systems that contain α+ß' phases in their microstructures are called duplex brasses. It is believed [11, 12] that an increase in the percentage of the ß' phase (which has an ordered body-centered cubic (BCC) structure) in the microstructure can lead to an improvement in the machinability of the alloy. Several researchers have made efforts to augment the ß' phase fraction in the microstructure to produce leadless free-cutting brasses by the addition of Si [11, 13], Sn [14] or heat treatment regimens [12]. Vilarinho et al. [15] observed that the addition of Al to a 60Cu-40Zn brass caused the cutting and feed forces to increase due to an increase in the fraction of ß' phase in the microstructure. They also found that the ß' phase can aid chip fragmentation only if the lead is present in the microstructure. This conclusion was in contrast to prior viewpoints [11-13].

Machining is one of the manufacturing processes that is affected by the properties of the workpiece material and cutting conditions (cutting speed, feed rate and depth of cut) [16]. In this paper, the effect of the addition of Al and Si on the microstructure, mechanical properties and machinability of 65Cu-35Zn brass is investigated. More specifically, the role of ß' phase, hardness, UTS and toughness in the machinability of Al and Si brass samples have been studied.

2.EXPERIMENTAL PROCEDURE

Brass alloys with 0, 0.83, 1.87, 2.28 and 3.62 wt% Si or 0, 1.89, 3.65 and 4.72 wt% Al were prepared in a resistance-heated furnace by adding high purity commercial Si and Al to 65Cu-35Zn alloy. The alloy was melted and heated to 1020 °C while covered with borax flux to prevent the oxidation of zinc during the process. The liquid alloys were then poured into cylindrical sand molds with a height of 200 and a diameter of 30 mm and were allowed to solidify and cool to room temperature. The composition of the resulting alloys, determined by mass spectroscopy, is shown in Table 1.

A specimen was cut from the bottom of each casting and was ground carefully to obtain a flat surface. The specimens cut from samples B, S1, S2, S3, and A1 were electro-polished (15 s at 27 V) and electro-etched (4 s at 1 V) with standard phosphoric acid using a Struers LectroPol-5 device. The specimen from sample S4 was ground, polished to 1 µm and etched using 2 vol% Nital etchant. Samples A2 and A3 were ground, polished to 1 µm and etched by 2.5 g Fe_2O_3 + 25 mL HCl + 50 mL H_2O.

In order to identify the phases formed during the solidification, X-ray diffraction (XRD, Xpert) was conducted. Microscopic investigations were carried out using a LEICA DMLM light optical microscope and a Camscan scanning electron microscope (SEM) fitted with an Oxford Inca EDX for microanalysis. Determination of the phase fractions was carried out using ImageJ 1.50f software. A linear intercept method was used on the optical micrographs to estimate the average grain size.

The Vickers micro-hardness test (MH3 micro-hardness tester) was utilized in order to determine the hardness of each phase in different samples. Micro-hardness tests were measured under a load of 50 mg for 15 s. The macro-hardness of the whole of the sample was also measured using the Brinell hardness method under a load of 62.5 kN for 60 s.

Tensile testing of the alloys was carried out using a GOTECH GT-7001-LC tensile test machine in accordance with the ASTM E8 standard [17] at ambient temperature. The tensile specimens were round with a diameter of 6 mm and a gauge length of 30 mm and were tested with a uniform rate of 5 mm min^{-1}. The data were collected in the form of load-extension and were then converted into engineering stress-strain curves using standard equations.

A TN50A lathe machine was used for the machining operation. The machining tests were carried out using no lubricant and DNMG 150608-PM inserts with the grade of YBC351. The insert is indexed based on ISO 1832. The cutting forces (i.e., main cutting force, thrust force, and feed force) were measured by a piezoelectric dynamometer KISTLER 9257B. The experiments were conducted at a feed rate of 0.11 mm rev^{-1}, cut depth of 0.5 mm and various cutting speeds of 33.4, 47, 66.8 and 94 m min^{-1}. The experiments were repeated three times for each machining condition. All tests were carried out under the rake angle of 0^o.

3.RESULTS

3.1.Microstructural Analysis and Phase Characterization

Fig. 1a shows the microstructure of the base yellow brass (sample B). The lighter and darker phases were identified by the XRD pattern shown in Fig. 2a to be α and β', respectively. The α phase was a solid solution of Zn in Cu with a face-centered cubic (FCC) structure, and β' was an ordered intermetallic compound with an approximate stoichiometry of CuZn which formed from the disordered β when the alloy was cooled below 460 °C [18]. Fig. 1b shows a higher magnification of this sample which demonstrates

Table1. Chemical composition of the as-cast samples

Sample	Cu	Zn	Si	Al	Ni	Fe	Pb
B	65.4	34.52	0	0	0.04	0.02	0.02
S1	66.07	33.01	0.83	0	0.05	0.02	0.02
S2	64.97	33.07	1.87	0	0.05	0.02	0.02
S3	64.69	32.94	2.28	0	0.05	0.02	0.02
S4	64.34	31.96	3.62	0	0.03	0.03	0.02
A1	62.92	35.1	0	1.89	0.04	0.03	0.02
A2	61.01	35.26	0	3.65	0.04	0.03	0.01
A3	60.54	34.66	0	4.72	0.04	0.03	0.01

[DOI: 10.22068/ijmse.16.2.21]

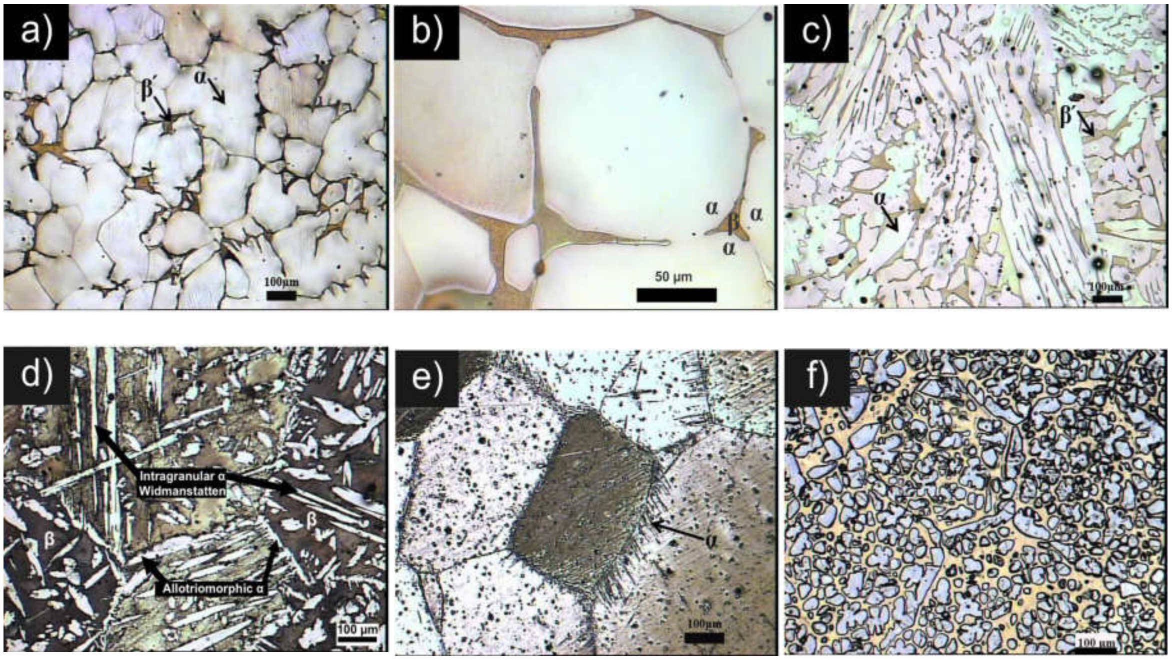

Fig. 1. Optical micrographs of the Si alloyed samples: (a) base metal, (b) higher magnification of (a), samples (c) S1 (0.83 Si), (d) S2 (1.87 Si), (e) S3 (2.28 Si) and (f) S4 (3.62 Si)

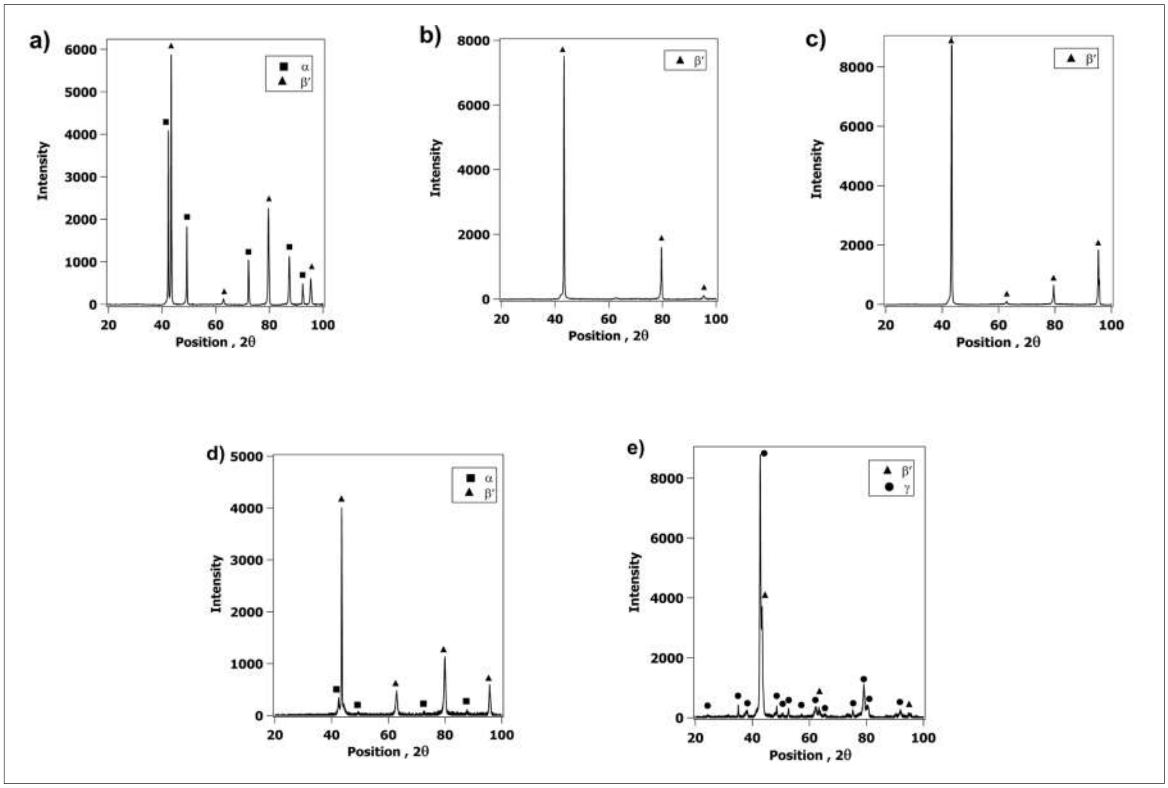

Fig. 2. XRD patterns obtained from samples (a) B, (b) S1, (c) S2, (d) S3 and (e) S4

[DOI: 10.22068/ijmse.16.2.21]

the β phase has nucleated in the α matrix at the grain boundaries, preferably at grain edges (three-grain junctions). The microstructure of sample S1 (containing 0.83 wt% Si) is shown in Fig. 1c. The α and β' phases formed a typical basket-weave microstructure. The XRD peaks corresponding to the β' phase obtained from this sample (shown in Fig. 2b) became larger than those obtained from sample B.

The microstructures of samples S2 and S3 (with Si content of 1.87 and 2.28 wt%, respectively) are shown in Figs. 1d and 1e, respectively. The XRD spectra obtained from these two samples, shown in Figs. 2c and 2d, respectively identified the lighter and darker phases in Fig. 1d to be α and β', respectively. In Fig. 1e, the small needle-like phase was identified to be α which nucleated at the boundary of the β' grains. The XRD spectra also showed that the intensity of the α phase decreased as the Si content of the alloy increased. The α phase had a Widmanstätten morphology in these two samples. The Widmanstätten precipitates had an intergranular morphology in sample S2 while they formed a needle-like structure at the grain boundaries in sample S3. More specifically, in sample S2 the Widmanstätten α plates nucleated and grew both at the grain boundaries and inside the grains (Fig. 1d), whereas in sample S3 this phase (which formed about 29% of the microstructure) was observed only at the grain boundaries (Fig. 1e).

Figs. 1f and 2e show the microstructure and the XRD spectrum, respectively, obtained from sample S4, which had a high Si content of 3.62 wt%. This microstructure consisted of globular γ phase dispersed almost homogeneously in the β' matrix. The γ phase was an intermetallic with a stoichiometric formula of Cu5Zn8 [19].

The micrograph of sample A1 with 1.89 wt% Al containing Widmanstätten precipitates with intergranular morphology and the XRD pattern of the sample are depicted in Figs. 3a and 4a. The Widmanstätten structure contained randomly oriented plates. Such microstructure has been observed previously [20].

Microstructures of the alloys containing 3.65 and 4.72 wt% Al (samples A2 and A3) contained ß' phase with a hexagonal structure (Figs. 3b and 3c). The XRD patterns obtained from these samples are also illustrated in Figs. 4b and 4c.

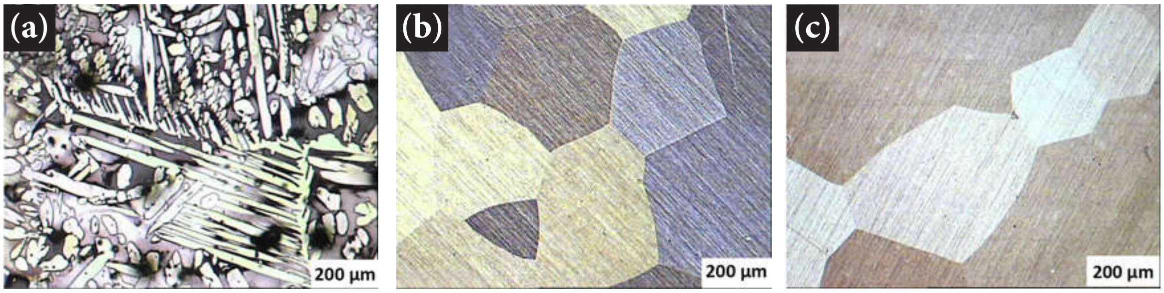

Fig. 3. Optical micrograph of the Al alloyed samples (a) A1 (1.89 Al), (b) A2 (3.65 Al), and (c) A3 (4.72 Al)

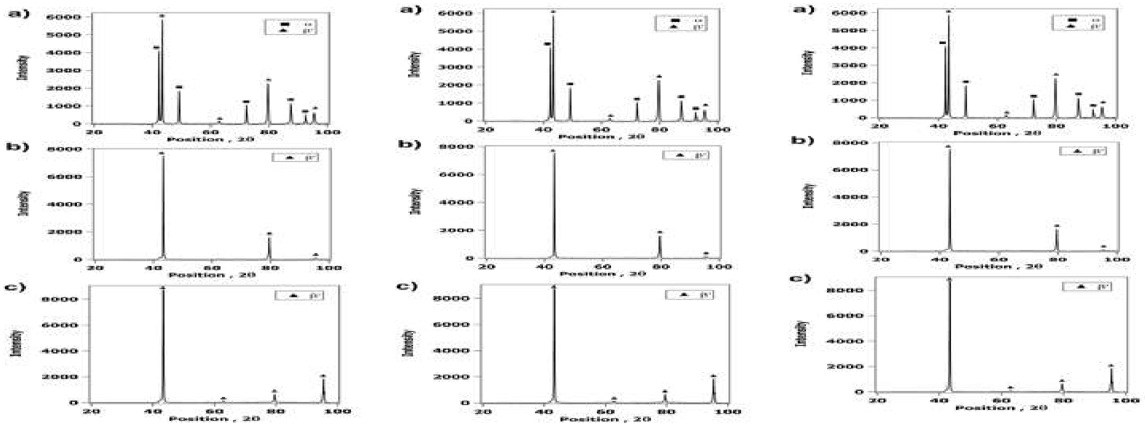

Fig. 4. XRD patterns obtained from samples (a) A1, (b) A2 and (c) A3

[DOI: 10.22068/ijmse.16.2.21]

The effect of Si and Al on the fraction of phases formed during the solidification is summarized in Figs. 5 and 6, respectively. The fraction of α phase decreased and that of β' phase increased as the concentration of Si in the alloy increased from 0 to 2.28 wt%. The fraction of α phase decreased to zero and that of γ phase increased to 68% when the Si content of the alloy increased to 3.62 wt% (sample S4). Adding 1.89 wt% Al to the base brass (sample A1) increased the β' phase fraction from 15 to 57% and when the concentration of Al increased to 3.65 (sample A2) or higher (sample A3) the whole of the microstructure consisted of β' phase.

The effect of Si and Al content on the average diameter of the grains (ADG) is shown in Figs. 7 and 8, respectively. For silicon brass alloys, the ADG showed a rapid decrease from about 57 µm to about 11 µm as the Si content of the alloy increased from 0 to 1.87 wt%. A further increase in the Si content caused this parameter to increase again to about 20 µm for the alloy that contained 3.62 wt% Si. For aluminum brass alloys, the ADG decreased with the addition of 1.89 wt% Al. The single-phase samples A2 and A3 showed an increase in their ADG to about 294 and 341 µm, respectively.

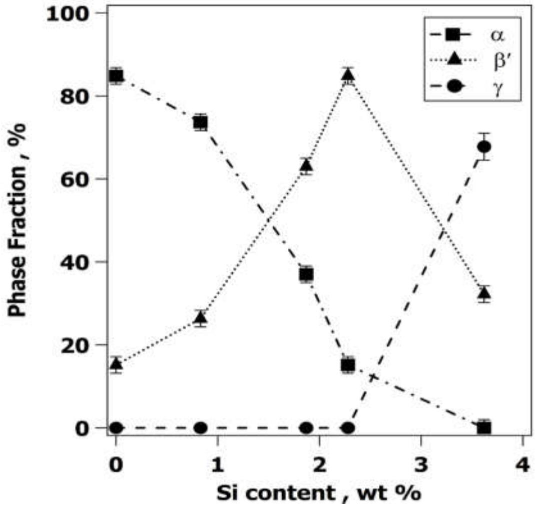

Fig. 5. Effect of Si on the fraction of phases formed during solidification

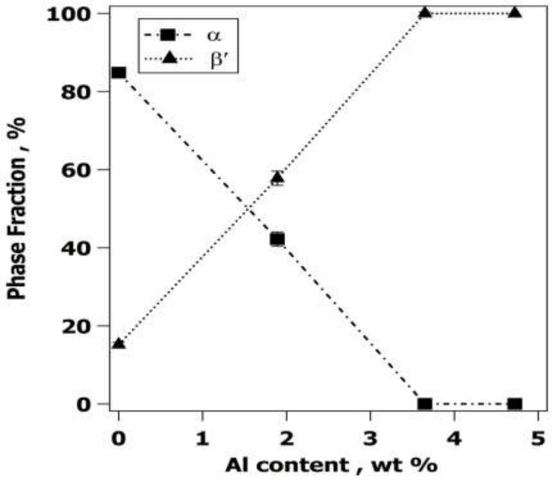

Fig. 6. Effect of Al on the fraction of phases formed during solidification

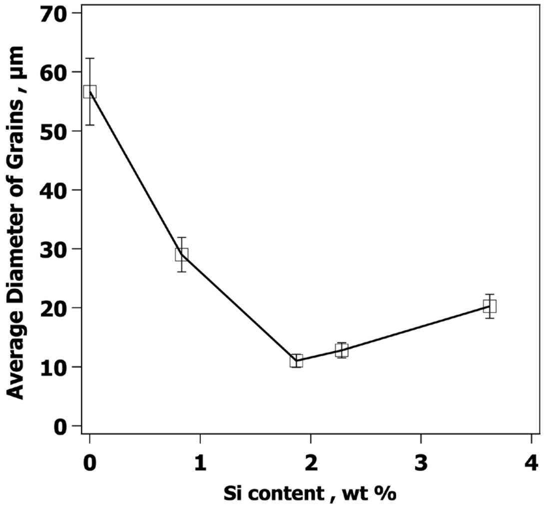

Fig. 7. Effect of Si addition on the average diameter of grains for Si-added samples

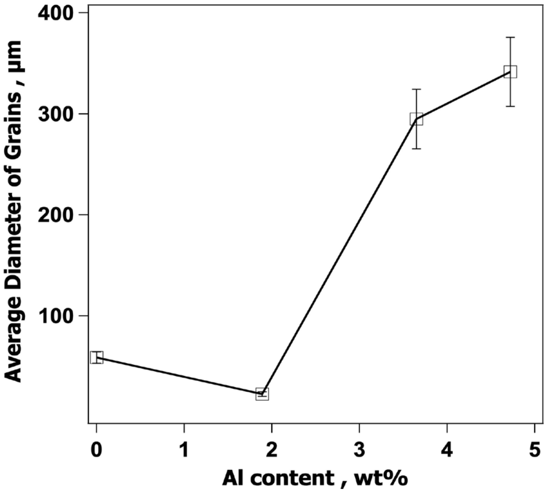

Fig. 8. Effect of Al addition on the average diameter of grains for Al-added samples

3.2. Mechanical Properties

The data obtained from the hardness tests are shown in Fig. 9. The hardness of the base brass was 76 HB, which increased almost linearly to about 293 HB (almost four folds) as the Si content of the alloy increased from 0 to 3.62 wt%. The increase in the Al content of the alloy also increased the hardness of the samples with an almost linear trend, but with a more gradual slope. The hardness increased to about 142 HB as the Al content of the alloy increased to about 4.72 wt%.

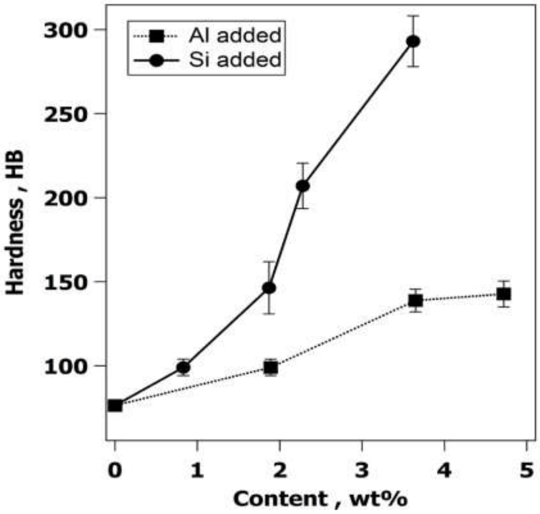

Fig. 9. Effect of Al and Si on the Brinell hardness of the alloyed brass samples

The hardness of each phase for samples containing various amounts of Si and Al is shown in Fig. 10. It is obvious that the hardness of the various phases is quite different. The hardness of β' phase (118 – 187 HV) was more than that of α (75 – 100 HV) and γ was measured to be the hardest phase (454 HV). This Figure also shows that the hardness of α and β' phases increased as the Si or Al content of the alloy increased. However, compared to Al, the addition of Si had a more dramatic effect on the increase in the hardness of the phases.

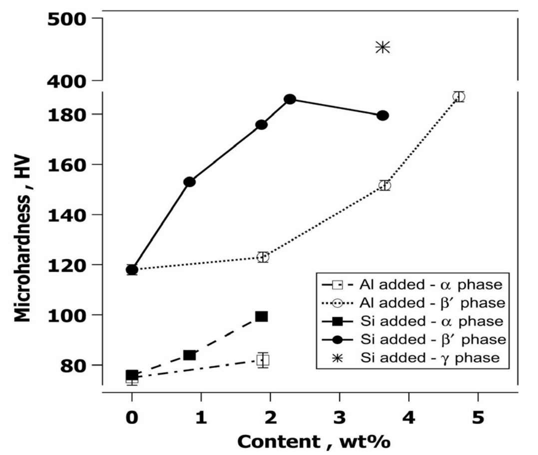

Fig. 10. Effect of Si and Al addition on the internal hardness of each phase

The effect of Si and Al addition on the ultimate tensile strength (UTS), elongation, toughness and yield stress of the samples is depicted in Fig. 11. The addition of Si up to 1.87 wt% caused the UTS of the sample to increase from 302 to 508 MPa. This mechanical property decreased sharply when more Si was added to the alloy and reached to 110 MPa for sample S4 which contained 3.62 wt% Si. The addition of Al to the base brass, up to 3.65 wt%, caused the UTS of the sample to increase almost linearly from 302 to 594 MPa and remained almost the same when the Al content increased to 4.72 wt%. The trend in the change of yield stress with the addition of Si and Al on the yield stress of the alloy was the same as that of UTS.

The elongation of the samples decreased as the concentration of Si (up to 2.28 wt%) or Al (up to 3.65 wt%) in the alloy increased. This property did not change significantly when more Si or Al was added to the alloy. Compared to Al, the rate of decrease in the elongation of the samples was more dramatic when Si was added to the alloy. The toughness of the alloy did not change significantly up to 0.83 wt% Si or 1.89 wt% Al. This property decreased sharply when more Si or Al was added to the alloy, up to 2.28 and 3.65 wt%, respectively, but did not change significantly again when the concentration of these two alloying elements increased further. Similar to the case of elongation, compared to Al, the addition of Si had a more significant effect on the decrease in the toughness of the alloy.

[DOI: 10.22068/ijmse.16.2.21]

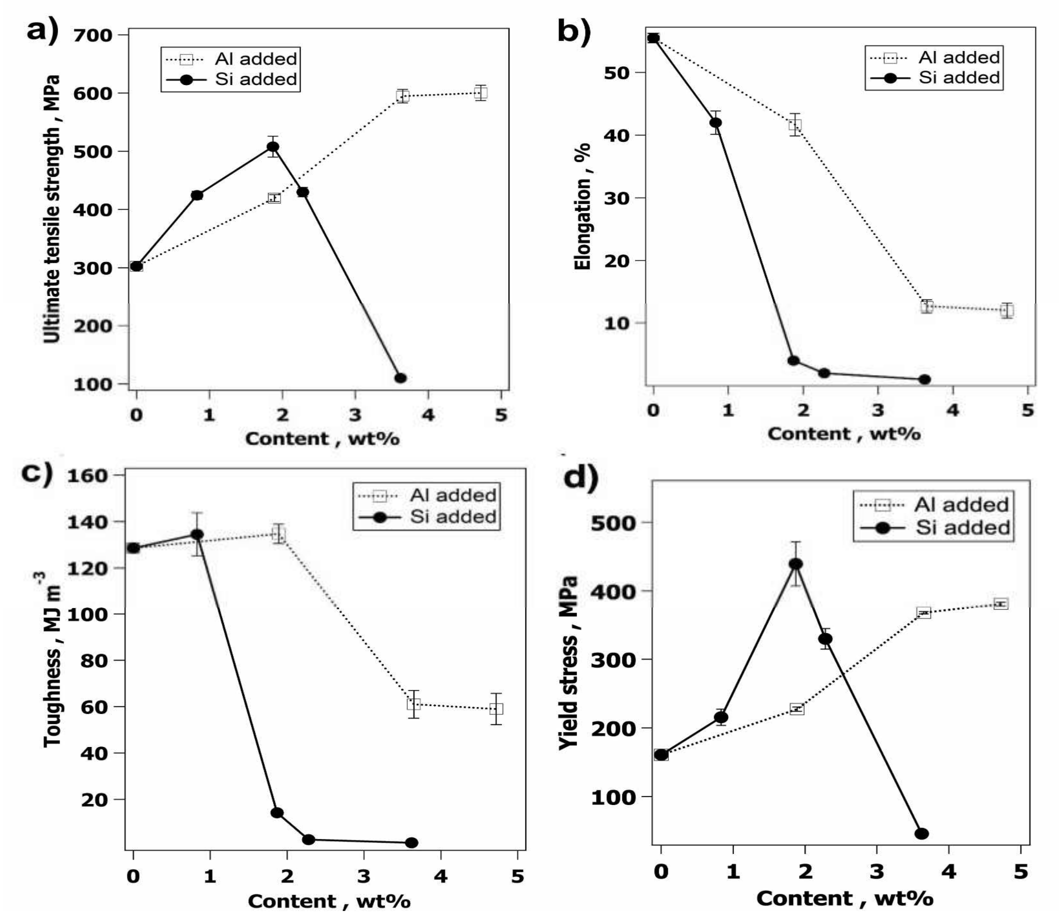

Fig. 11. Effect of Si and Al content on the (a) UTS, (b) elongation, (c) toughness and (d) yield stress of the samples

3.3. Machinability Investigations

The effect of cutting speed on the cutting force components (main cutting force, thrust force and feed force) of different samples with various concentrations of Si and Al is shown in Figs. 12 and 13, respectively. The addition of Si, up to 1.87 wt%, caused the main cutting force for all cutting speeds to decrease. This parameter increased again when more Si (up to 3.62 wt%) was added to the alloy. Sample S4 with 3.62 wt% Si caused the main cutting force to be less than that of the base metal only at cutting speeds of 47 m min^{-1} or lower. The main cutting force stayed at the same level as the cutting speed variation for samples S2 and S3 with 1.87 and 2.28 wt% Si, respectively. Additions of Si to the base brass resulted in an increase in the thrust and feed forces in all cutting speeds. These two forces increased further as more Si was added to the alloy.

Among the Al-added samples, sample A1, with 1.89 wt% Al, was the only sample that showed the main cutting force lower than that of the base brass. Samples A2 and A3, which had microstructures consisting of only β' phase, required relatively high main cutting forces during the machining. The main cutting force for samples B, A2 and A3 decreased as the cutting speed increased, whereas this parameter increased in sample A1 with an increase in cutting speed.

The thrust and feed forces showed a small increase when 1.89 wt% Al was added to the alloy. In samples formed by single β' (i.e., samples A2 and A3) the thrust and feed forces increased significantly compared to those of samples B and S1.

[DOI: 10.22068/ijmse.16.2.21]

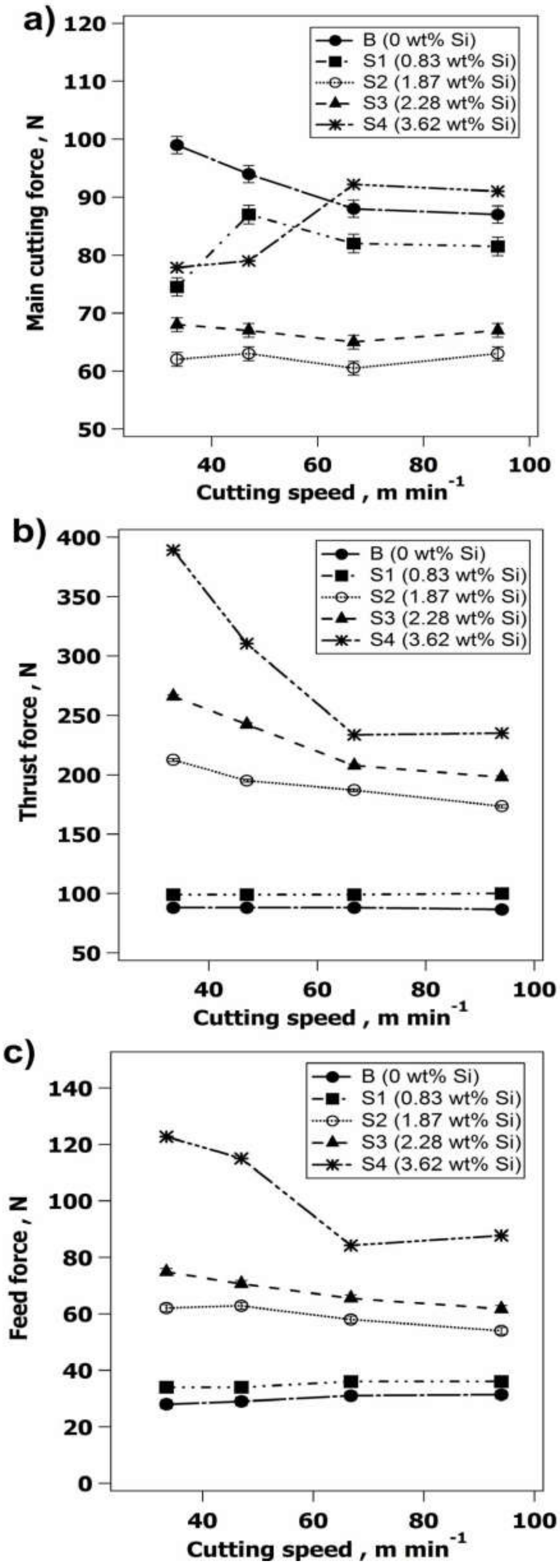

Fig. 12. Variation of cutting forces with cutting speed for Si-added samples

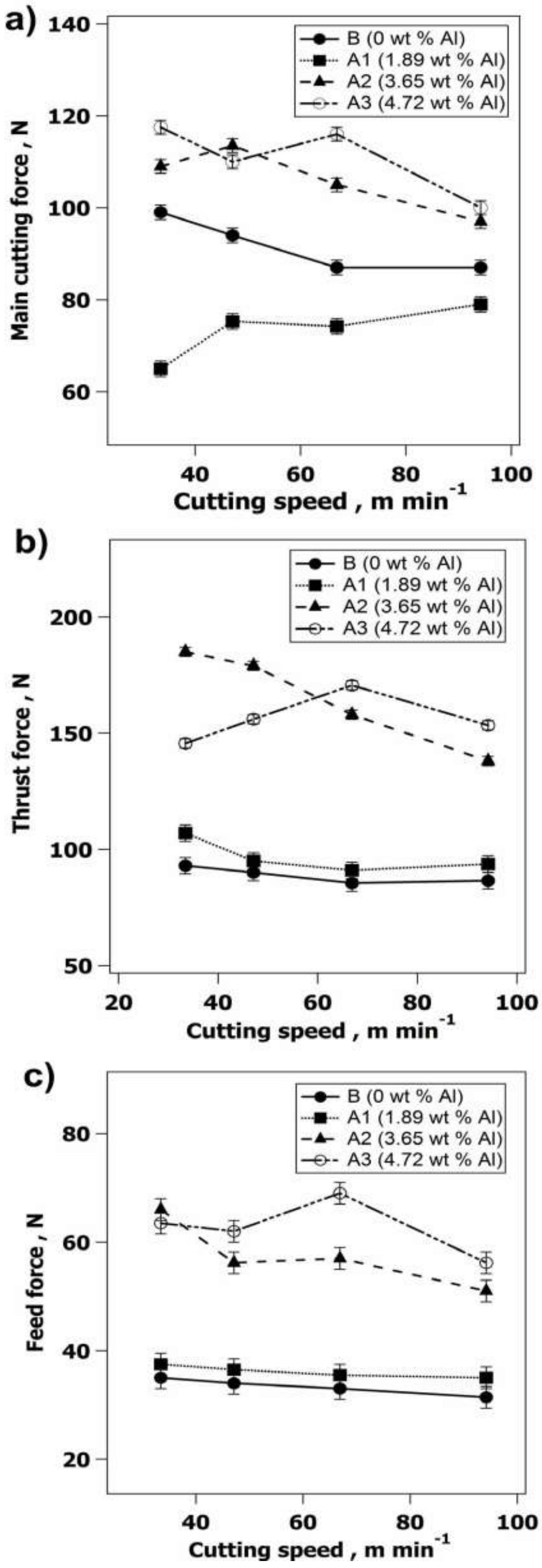

Fig. 13. Variation of cutting forces with cutting speed for Al-added samples

[DOI: 10.22068/ijmse.16.2.21]

Fig. 14 shows the SEM micrographs of the chips obtained from machining samples S1 and S2 with a cutting speed of 94.2 m min^{-1}. Both chips had saw-teeth morphology. The teeth of the chips from sample S1 were less regular than those of sample S2. Moreover, during the machining, the chips from sample S2 were observed to break more easily than those of sample S1.

The micrographs of the chips obtained from sample A1 at cutting speeds of 33.4 and 94.2 m min^{-1} are shown in Fig. 15. At a cutting speed of 33.4 m min^{-1}, the morphology of the chips became serrated along the free side. However, at a cutting speed of 94.2 m min^{-1}, the chips became more continuous during the machining operation.

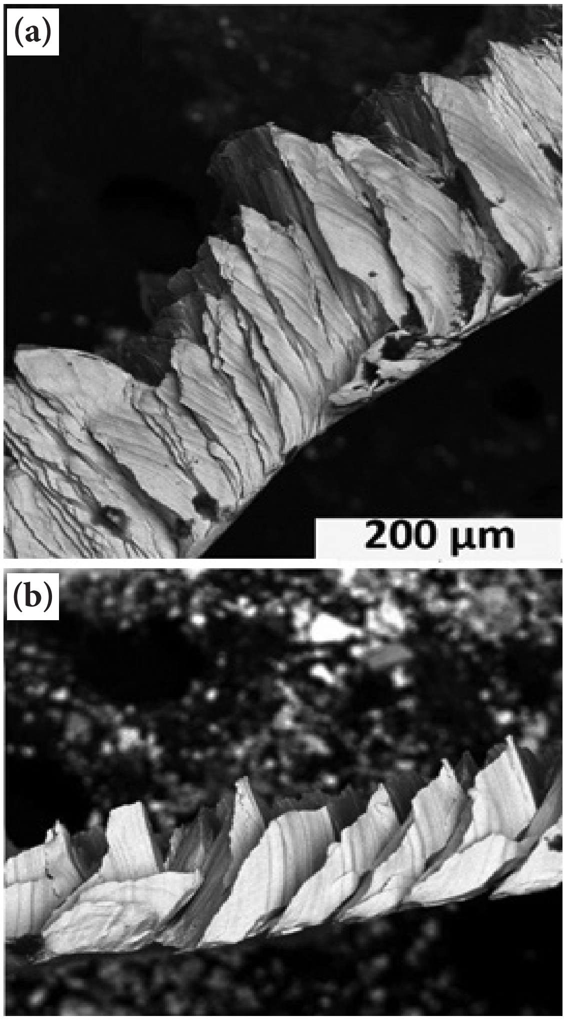

Fig. 14. SEM micrographs of the chips obtained from machining with a cutting speed of 94.2 m min^{-1} from (a) sample S1 and (b) sample S2

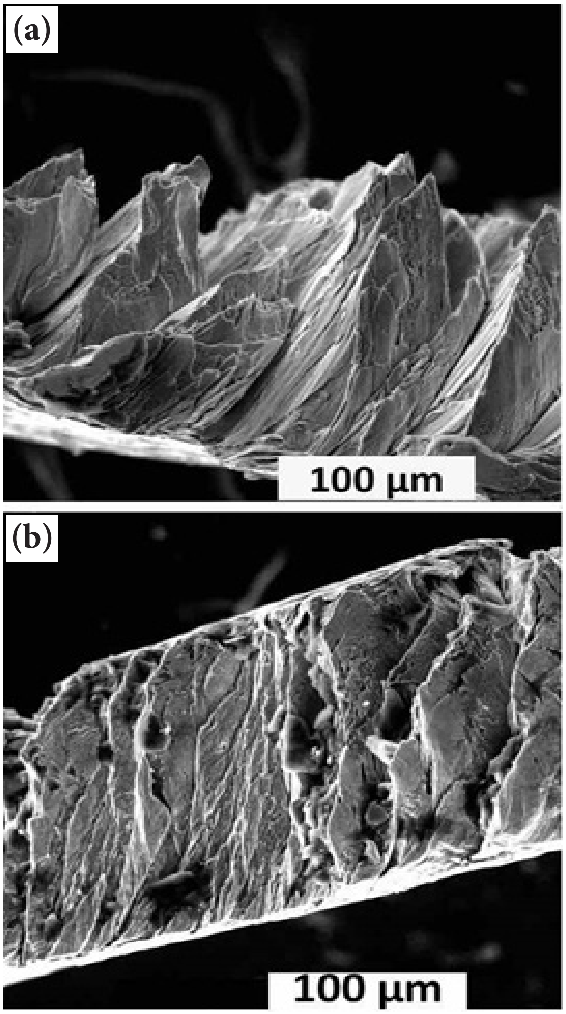

Fig. 15. SEM micrograph of the chips obtained from sample A1 machined with a cutting speed of (a) 33.4 and (b) 94.2 m min^{-1}

4. DISCUSSION

The main cutting force is the most important force component during turning operation. This force spends most of the cutting power since most of the relative motion of the tool and the work-piece is in the direction of cutting. There is no movement in the direction of the thrust force and the movement in the direction of the feed force is negligible compared to the cutting direction. However, thrust and feed forces cause the tool to bend and torsional moments to occur during the machining. These forces, therefore, can induce shear stresses in the tool and affect its life.

[DOI: 10.22068/ijmse.16.2.21]

Machining operations bring about high strain rates in the range of 10^3-10^7 s^{-1}. At these high strain rates, the velocity of dislocations throughout the lattice and the density of these defects increase, resulting in a significant increase in the temperature [21]. In this case, no heat can transfer in a short time and material starts to deform locally in narrow bands which are known as adiabatic shear bands [22].

The source of the shear localization is the presence of inhomogeneity in the microstructure of the material, which can result in the non-uniform generation of stress and strain during deformation [23]. The inhomogeneity in the microstructure arises from the presence of particles of a second phase, the inclusion-matrix interface, grain boundaries [24] and bifilms produced during casting operation [25]. These irregularities in the microstructure can give rise to stress concentration and void formation.

Under severe dynamic loading, the voids grow and coalesce along with the shear bands inducing void sheets [24]. Having reached a critical value, the void sheets lead to micro-cracks aligning in the direction of shear [26]. Depending on the nature of the material and the intensity of the compressive stress exerted by the tooltip, micro-cracks can display two behaviors: 1) propagate and connect with each other causing fracture to form on the free side of the chips and the formation of catastrophic shear chips (see Figs. 14b and 15a) or 2) to be closed by high compressive stress formed from the tooltip or locally welded due to the high heat generation, causing the formation of continuous chips (see Figs. 14a and 15b) [26, 27].

Besides the presence of shear bands, the brittleness of the material can play an important role in the machinability of metals. The concentration of elements added to samples S2 and A1 was almost the same (1.87 wt% Si and 1.89 wt% Al, respectively). However, Fig. 11c indicates that sample S2 (with the toughness of about 14 MJ m^{-3}) was much more brittle than sample A1 (with the toughness of about 135 MJ m^{-3}). The more fragile nature of sample S2 caused this sample to require a smaller main cutting force for machining compared to sample A1 (an average of about 62 and 73 MPa, respectively (see Figs. 12a and 13a).

The cutting speed also influences the fracturing tendency of the material. The chips obtained from samples A1 and S1 showed better fracturing behavior (i.e., less main cutting force required) at lower cutting speeds (Figs. 12a and 13a). These two samples had similar hardnesses (Fig. 9) and very close ultimate tensile stresses, elongations and toughnesses (Fig. 11). They also showed a similar trend in terms of the main cutting force required during machining with cutting speed variation (see Figs. 12 and 13). Samples A2 and A3, which formed from a single β' phase, could behave more homogeneously under deformation due to the lack of the presence of the second phase particles. They had a low potential for the void formation and fracturing. However, at high cutting speeds, which is equivalent to high strain rates (due to faster material deformation), more shear bands could form and thus thermal softening could take place, which in turn resulted in a decrease in the main cutting force needed for the machining of these samples.

Thermal softening was also observed in sample B. In this sample (with 15% β'), the β' phase nucleated and grew only at the α grain boundaries (see Figs. 1a and 1b). Therefore, the homogeneity of the microstructure was higher than that of samples S1 and A1. For these two samples, the second phase (β') nucleated and grew both at the grain boundaries and the interior of the grains, creating more interfaces between the phases.

Widmanstäetten structures have low toughness and cause the microstructure to become brittle [28]. The α phase in sample S2 had an intergranular Widmanstäetten structure (see Fig. 1d) and hence had a lower toughness compared to sample S1 which had a basket-weave microstructure of α + β', Fig. 1c (about 14 and 135 MJ m^{-3}, respectively, see Fig. 11c). The deterioration of mechanical properties became more severe when the Widmanstäetten structures nucleated and grew along the grain boundaries [29].

It has also been said that the critical strain for beginning the formation of shear bands is less for lamellar microstructures compared to single phase microstructures [30]. Samples S2 and A1 were formed from Widmanstäetten α plates in β' matrix and had lamellar microstructures. This kind of microstructure is more sensitive to the formation of shear bands, which can lead to a low main cutting

[DOI: 10.22068/ijmse.16.2.21]

[DOI: 10.22068/ijmse.16.2.21]

force, especially at low cutting speeds.

The results of this study showed that sample S3, with Widmanstäetten needles along the grain boundaries, had better machinability compared to the base alloy which had no Widmanstäetten structure.

According to the data of this research, the improvement in machinability of the Si alloyed samples could continue up to a Si content of 1.87 wt% in which the UTS had the highest value. Past this critical concentration, the machinability became worse due to a drop in the UTS of the material. Increasing hardness led to a decrease in the main cutting force up to 146 HB. After this point, the increase in the hardness of the material could not help the machinability due to a decrease in the UTS.

It is suggested in the literature [15, 31] that the β' phase enhances the breakage of chips and improves machinability. This research, however, found that the percentage of β' phase in the microstructure is not the only structural factor affecting machinability. Samples A2 and A3, which consisted of only β' phase, required higher main cutting forces, thrust force and feed force for machining compared to sample A1 in which the β' phase consisted about 58% of the microstructure (see Fig. 6).

The results of this study suggest that not only the presence of brittle phases (such as β' phase) in the microstructure is essential for good machinability, but also the morphology and hardness of the phases involved have a significant effect in this regard. For Si brass alloys, sample S1 containing about 26% β' phase and sample S4 containing 32% β' phase and 68% brittle γ phase in their microstructures could not improve the machinability remarkably (see Fig. 12). However, samples S2 and S3 containing phases with Widmanstäetten morphologies improved the machinability significantly.

Overall, the authors believe that a fine-grained α+ß' microstructure can achieve better machinability due to the presence of more inhomogeneity in the microstructure which results in better fracturing behavior through the void formation mechanism.

5. CONCLUSIONS

1. A duplex brass (obtained from both Si or Al addition) with randomly oriented α plates in β' matrix was found to have better machinability compared to the other microstructures.
2. Both Si and Al initially enhanced the UTS and toughness of the brass samples, which led to an improvement in the machinability by reducing the main cutting force required for machining. The role of Si in the reduction of the main cutting force and chip breaking was more significant than Al.
3. The results of this study suggest that not only the presence of brittle phases (such as β' phase) in the microstructure is essential for good machinability, but also the morphology and hardness of the phases involved have a significant effect in this regard
4. The addition of 1.87 wt% Si could decrease the main cutting force between 28-37 percent depending on the cutting speed. The positive role of Si continued to the point that UTS had the highest value.
5. The addition of 1.89 wt% Al decreased the main cutting force between 10-34 percent. The positive role of Al continued to the highest value of toughness of the alloy.

REFERENCES

1. Lee, D. B. and Moon, J. J., "The effect of small additions of Zr, Cr, Mg, Al, and Si on the oxidation of 6:4 brass." Met. Mater. Int., 2002, 8, 327-332.
2. Mohammadnejad, M., Ehteshamzadeh, M. and Soroushian, S., "Effect of annealing on microstructure and corrosion performance of ADB and ALB alloys." Iran. J. Mater. Sci. Eng., 2014, 11, 1-13.
3. Pugacheva, N. B., Pankratov, A. A., Frolova, N. Y. and Kotlyarov, I. V., "Structural and phase transformations in α + β brasses. Russ." Metall., 2006, 3, 239-248.
4. Asanovi, V., Deliji, K. and Jaukovi, N., "Isothermal decomposition of the β' phase in Cu-Zn-Al shape-memory alloys." Materiali in Tehnologije, 2006, 40, 153-156.
5. Chen, B., Liang, C., Fu, D. and Ren, D., "Corrosion behavior of Cu and the Cu-Zn-Al shape memory alloy in simulated uterine fluid." Contraception, 2005, 72, 221-224.
6. Fricoteaux, P. and Rousse, C., "Nanowires of Cu–

Zn and Cu–Zn–Al shape memory alloys elaborated via electrodeposition in ionic liquid." J. Electroanal. Chem., 2014, 733, 53-59.

7. García, P., Rivera, S., Palacios, M. and Belzunce, J., "Comparative study of the parameters influencing the machinability of leaded brasses." Eng. Fail. Anal., 2010, 17, 771-776.
8. Schultheiss, F., Johansson, D., Linde, M., Tam, P. L., Bushlya, V., Zhou, J., Nyborg, L. and Ståhl, J. E. "Machinability of CuZn21Si3P brass." Mater. Sci. Technol., 2016, 32, 1744-1750.
9. Schultheiss, F., Johansson, D., Bushlya, V., Zhou, J., Nilsson, K. and Ståhl, J. E., "Comparative study on the machinability of lead-free brass." J. Cleaner Prod., 2017, 149, 366-377.
10. Nobel, C., Klocke, F., Lung, D. and Wolf, S., "Machinability enhancement of lead-free brass alloys." Procedia CIRP, 2014, 14, 95-100.
11. Doostmohammadi, H. and Moridshahi, H., "Effects of Si on the microstructure, ordering transformation and properties of the Cu60Zn40 alloy." J. Alloys Compd., 2015, 640, 401-407.
12. Toulfatzis, A. I., Pantazopoulos, G. A. and Paipetis, A. S., "Microstructure and properties of lead-free brasses using post-processing heat treatment cycles." Mater. Sci. Technol., 2016, 32, 1771-1781.
13. Alirezaei, M. and Doostmohammadi, H., "Microstructure evolution in cast and equilibrium heat-treated CuZn30-(Si) alloys. Int. J. Cast Met." Res., 2016, 29, 222-227.
14. Rajabi, Z. and Doostmohammadi, H., "Effect of Addition of Tin on the Microstructure and Machinability of α-Brass. Mater." Sci. Technol., 2018, 34.
15. Vilarinho, C., Davim, J. P., Soares, D., Castro, F. and Barbosa, J., "Influence of the chemical composition on the machinability of brasses." J. Mater. Process. Technol., 2005, 170, 441-447.
16. Ånmark, N., Karasev, A. and Jönsson, P. G., "The effect of different non-metallic inclusions on the machinability of steels." Materials (Basel), 2015, 8, 751-783.
17. ASTM E8 / E8M-11, "Standard test methods for tension testing of metallic materials." ASTM International: West Conshohocken, PA, USA, 2011.
18. Davis, J. R., "ASM Specialty Handbook: Copper and Copper Alloys, ASM international," Materials Park, OH, USA, 2001, 34-35.
19. Wang, J., Xu, H., Shang, S., Zhang, L., Du, Y., Zhang, W., Liu, S., Wang, P. and Liu, Z. K., "Experimental investigation and thermodynamic modeling of the Cu–Si–Zn system with the refined description for the Cu–Zn system." Calphad, 2011, 35, 191-203.
20. Hsieh, C. C., Wang, J. S., Wu, P. T. Y. and Wu, W., "Microstructural development of brass alloys with various Bi and Pb additions." Met. Mater. Int., 2013, 19, 1173-1179.
21. Li, J., Guo, H. and Zhou, P., "Experimental study and analysis of the dynamic mechanical properties of aluminium bronze." Journal of Mechanical Engineering, 2015, 61, 669-679.
22. Williams, J. A., "Deformation diagrams of chip forming mechanisms." J. Mater. Sci., 1977, 12, 621-624.
23. Hofmann, U. and El-Magd, E., "Behaviour of Cu-Zn alloys in high speed shear tests and in chip formation processes. Mater." Sci. Eng., A, 2005, 395, 129-140.
24. Sabih, A. and Nemes, J. A.," Internal ductile failure mechanisms in steel cold heading process." J. Mater. Process. Technol., 2009, 209, 4292-4311.
25. Dørum, C., Hopperstad, O. S., Berstad, T. and Dispinar, D., "Numerical modelling of magnesium die-castings using stochastic fracture parameters." Eng. Fract. Mech., 2009, 76, 2232-2248.
26. Komanduri, R. and Brown, R. H., "On the mechanics of chip segmentation in machining." Journal of Engineering for Industry, 1981, 103, 33-51.
27. Morehead, M. D., Huang, Y. and Luo, J., "Chip morphology characterization and modeling in machining hardened 52100 steels." Machining Science and Technology, 2007, 11, 335-354.
28. Liu, Y., "Research of the formation mechanism of widmanstätten ferrite in 30Mn2 steel." Emerging Computation and Information teChnologies for Education, 2012, 146, 695-699.
29. Gil, F. J., Ginebra, M. P., Manero, J. M. and Planell, J. A., "Formation of α-widmanstätten structure: Effects of grain size and cooling rate on the widmanstätten morphologies and on the mechanical properties in Ti6Al4V alloy. "J. Alloys Compd., 2001, 329, 142-152.
30. Yang, Y., Li, X. M., Tong, X. L., Zhang, Q. M. and Xu, C. Y., "Effects of microstructure on the adiabatic shearing behaviors of titanium alloy." Mater. Sci. Eng., A, 2011, 528, 3130-3133.
31. Pantazopoulos, G. A. and Toulfatzis, A. I., "Fracture modes and mechanical characteristics of machinable brass rods." Metallography, Microstructure, and Analysis, 2012, 1, 106-114.